Received June 3, 2021, accepted June 21, 2021, date of publication June 25, 2021, date of current version July 5, 2021.

Digital Object Identifier 10.1109/ACCESS.2021.3092335

Enabling User Grouping and Fixed Power Allocation Scheme for Reconfigurable Intelligent Surfaces-Aided Wireless Systems

ANH-TU LE[1], NHAT-DUY XUAN HA[1], DINH-THUAN DO[2], (Senior Member, IEEE), ADÃO SILVA[3,4], (Member, IEEE), AND SUNEEL YADAV[5], (Member, IEEE)

[1]Faculty of Electronics Technology, Industrial University of Ho Chi Minh City, Ho Chi Minh City 700000, Vietnam
[2]Department of Computer Science and Information Engineering, College of Information and Electrical Engineering, Asia University, Taichung 41354, Taiwan
[3]Instituto de Telecomunicações (IT), University of Aveiro, 3810-193 Aveiro, Portugal
[4]Departamento de Eletrónica, Telecomunicações e Informática (DETI), University of Aveiro, 3810-193 Aveiro, Portugal
[5]Department of Electronics and Communication Engineering, Indian Institute of Information Technology Allahabad, Prayagraj 211015, India

Corresponding author: Dinh-Thuan Do (dodinhthuan@asia.edu.tw)

This work was supported by the Fundação para a Ciência e Tecnologia (FCT/MCTES) through national funds and co-funded EU funds under Project UIDB/50008/2020-UIDP/50008/2020. The work of Dinh-Thuan Do was supported by the Ministry of Science and Technology (MOST), Taiwan, under Grant MOST 110-2222-E-468-001.

This work did not involve human subjects or animals in its research.

ABSTRACT This paper considers a two-user downlink transmission in reconfigurable intelligent surface (RIS)-aided network over fading channels. Particularly, by employing user grouping and fixed power allocation scheme to enable non-orthogonal multiple access (NOMA) approach, RIS-aided network can significant benefit from NOMA. To highlight the advantages of RIS, we compare the system performance of NOMA-RIS and traditional orthogonal multiple access (OMA) based RIS. Main practical circumstances are carefully analyzed, such as, RIS with direct link, system without RIS, and imperfect phase shifts. More specifically, we consider a RIS-aided downlink network, where the base station communicates with a group of two users under assistance of RIS, which acts equivalently as relay. As key expectation, the RIS is efficiently designed to improve the performance of users. To evaluate the system performance, two main system performance metrics including outage probability and average capacity are studied by deriving new closed-form expressions. The goal is to find out which system parameters need to be adjusted to achieve the expected performance. The numerical results reveal that: i) *the outage probability and average capacity of considered NOMA-RIS aided wireless system outperforms the conventional NOMA network over fading channels*; ii) *with different power allocation factors assigned to users, the performance gap among two users can be adjusted to guarantee the fairness characteristic*; iii) *the number of reflecting elements in RIS has significant impact on the system performance of the considered NOMA-RIS system, which shows advantage of both RIS and NOMA compared with conventional OMA system.*

INDEX TERMS Reconfigurable intelligent surface, non-orthogonal multiple access, resource allocation.

I. INTRODUCTION

In recent years, reconfigurable intelligent surface (RIS) is recognized as a promising candidate to achieve high spectrum and energy efficiency in the wireless communications [1]. RIS contains reconfigurable reflecting elements in its planar surfaces which are passive and low-cost. The phase and/or amplitude for the incident signal in each element can be separately adjusted. For the highly efficient deployment of emerging techniques in sixth generation (6G) wireless networks, RIS has received focused attention owing to its significant capability of introducing a smart and controllable signal propagation environment with respect to enhance the spectrum utilization [2], [3], broadband connectivity and radio coverage [4]–[6].

In recent studies [7], [8], the weighted sum rate of all cell-edge users can be greatly enhanced by collaboratively designing the RIS elements in a downlink multicell scenario

The associate editor coordinating the review of this manuscript and approving it for publication was Prakasam Periasamy.

TABLE 1. Comparison of proposed system with related studies.

Context	Year	Proposed Scenario	NOMA	Impact of Direct Links	Performance Metrics	Fading Scenario
This Work	2021	RIS	Yes	Yes	Outage Probability and Ergodic Capacity	Rayleigh Fading
[5]	2020	RIS	Yes	No	Outage Probability and Throughput	Rayleigh Fading
[38]	2020	RIS	Yes	Yes	Outage Probability, Ergodic Capacity, Spectral Efficiency and Energy Efficiency	Nakagami-m Fading
[39]	2021	RIS	No	Yes	Outage Probability and Ergodic Capacity	Nakagami-m Fading
[40]	2021	RIS	Yes	No	Secrecy Outage Probability	Rayleigh Fading
[41]	2020	RIS	No	No	Outage Probability, Probability of SNR Gain and Delay Outage Rate	Rayleigh Fading

and precoders at multiple base stations (BSs). The work in [9] explored a downlink multiple-input-single-output (MISO) system with self-sustainable RIS in terms of optimal sum-rate as well as energy harvesting and power consumption (due to reflecting elements' phase shifter) at the RIS. In [10], the authors evaluated the minimal rate of cell-edge users by significantly improving the cooperative beamforming in joint processing coordinated multipoint downlink transmissions. The works [11], [12] studied downlink simultaneous wireless information and power transfer (SWIPT) coupled with transmit beamforming optimization in RIS-enabled network, without negotiating the quality-of-service (QoS) requirements. Besides, these results regarding wireless networks under various settings pointed RIS as a technology with great potentials. Besides, the brand-new RIS technology has also showed its potential in various wireless techniques, such as, non-orthogonal multiple access (NOMA), orthogonal frequency division multiplexing (OFDM), physical layer secure transmission, cognitive radio (CR), and mobile edge computing (MEC) [13]–[19].

A. RELATED WORK

To integrate RISs with existing wireless communications, multiple access techniques should also be considered. Since non-orthogonal multiple access (NOMA) can support multiple users in the same resource block (i.e., time, frequency, and code), therefore it is regarded as a promising technology to be integrated with RIS, forming a new approach referred as NOMA-RIS. To deploy NOMA in wireless networks, the transmitter sends superimposed signals to the receiver, and the receiver adopts a successive interference cancellation (SIC) technique for successful decoding of the signal [20]–[26]. As main benefits reported in [27]–[33], NOMA exhibits advances in terms of user fairness, sum rate, secrecy rate and outage probability, which can achieve considerable performance gains over traditional orthogonal multiple access (OMA).

The authors in [34] presented a two-user NOMA group without deteriorating the performance of the NOMA cell-center user. In particular, RIS approach and the joint transmission coordinated multipoint jointly deployed in order to improve the cell-edge user's performance. While joint transmission coordinated multipoint is implemented to eliminate the effects of inter-cell interference (ICI), the RIS is adopted to construct a strong combined channel gain at the cell-edge user. In such framework, a closed-form expression is derived for the ergodic capacity at the cell-edge user, and then the network spectral efficiency can be achieved. The study in [35] conducted NOMA downlink network by using a multi-cluster MISO setup, in which the BS needs RISs to assist the communication while all the destinations by exploiting passive beamforming. The main result is that the optimal transmit power can be obtained by jointly optimizing the reflection coefficient vector at the RISs and the active beamforming matrices at the BS. In [36], a MISO NOMA network was considered to maximize the energy efficiency of the users by designing joint deployment of phase shift and power allocation. The authors in [37] designed MIMO NOMA with a novel passive beamforming weight at RISs for simultaneously serving paired users. A signal cancellation based (SCB) design is adopted and the minimal number of RISs in both reflector and the diffuse scattering scenarios were evaluated. Table 1 summarizes and compares some of the discussed works.

We can point out many advances of such NOMA-RIS systems. Firstly, destination nodes in non-RIS NOMA networks rely on their channel conditions to usually order them. Secondly, the channels associated with RIS and the phase-shift matrix of RIS configuration are coupled with each other in RIS-aided NOMA networks. Thirdly, by intelligently reconfiguring the reflected signal propagation, RIS experiences a new way to improve the performance of current NOMA systems. Fourthly, by adjusting the RIS's phase shifts, the user fairness of RIS-aided NOMA systems can be highly maintained. More importantly, power-domain NOMA technology can be considered as an effort to empower user connectivity and the spectrum efficiency of non-NOMA RIS wireless networks. These prominent advances motivate us to

explore system performance analysis with respect to downlink NOMA-RIS systems.

B. OUR CONTRIBUTIONS

Motivated by the aforementioned studies [34]–[36], in this paper, we consider the two main performance metrics normally used in the NOMA-RIS systems to determine the necessary parameters, so that the performance gap among the two users can be adjusted. As mentioned, RIS is able of configuring the channels of the users by intelligently controlling the reflected signal amplitudes and phase shifts, and thus the user decoding order of non-RIS NOMA can be permuted by adjusting the RIS refection parameters to achieve better users' fairness performance in RIS-NOMA based systems. Specifically, theoretical closed-form expressions of outage probability and average capacity that can be used to efficiently configure these parameters so as to adjust the performance gap among the users, and thus increasing the user fairness. These expressions have not been derived yet for the considered downlink RIS-NOMA scenario and thus, in this work we aim to fill some of the gaps and derive closed-form expressions for both outage probability and ergodic capacity that allow to evaluate the impact of some parameters on system performance.

- We assume a RIS-NOMA aided downlink communication system, where the BS communicates with a dedicated group of users. To reduce the complexity of NOMA configuration, we adopt a fixed power allocation scheme and focus on a group of two users[1] since it was reported with acceptable performance [14]. Moreover, we consider system performance gap among the two users by allocating different power levels to the near and the far users.
- We derive the new closed-form expressions of outage probability and average capacity of the considered system. The aim is to show the trade-off between system performance and main parameters, such as, transmit signal to noise ratio (SNR) at the BS, power allocation coefficients, phase shift coefficient and channel gains.
- Three scenarios related to direct link, normal relay and RIS are studied to provide guidelines for implementation of NOMA-RIS in practice. The main results indicate that system benefits from the unique architecture with RIS and with normal relay, even with or without direct links. In particular, we consider several practical schemes in this study. We address how system parameters should be set to NOMA-RIS system to outperform the counterpart (cooperative NOMA). Although it is still hard to convey how NOMA-RIS cost in real deployment, but the advances obtained from RIS are enough to recommend RIS in real applications.

The rest of this paper is organized as follows. Section II presents the NOMA-RIS system model. Section III describes two main system performance metrics including outage probability and average capacity at Scheme I (NOMA with RIS) while Scheme II (NOMA without RIS) is considered as necessary benchmark represented in Section IV. The direct links are considered in term of two main system performance metrics in Section V (Scheme III). Simulation results are presented in Section VI to support and verify the mathematical derivations. We conclude this study by presenting main results in Section VII.

[1]Note that this work can readily be extended for the multiple users scenario.

TABLE 2. The symbols in considered systems.

Symbol	Description
x_i	The signal of D_i
P_i	The power allocation of D_i with $\sum_{i=1}^{2} P_i = 1$ and $P_2 > P_1$
P_S	The transmit power at base station
f_n and k_{ni}	The amplitudes of the channel gains and follows independent distributed Rayleigh distribution
f_{SD_i}	The channel between S and D_i and follows independent distributed Rayleigh distribution
d_{SD_i}	The distances from S to D_i
d_{SR}	The distances from S to RIS
d_i	The distances from RIS to D_i
α	The path-loss coefficient
θ_n and φ_n	The phases of the channel gains
n_i and n_{D_K}	The additive white Gaussian noise (AWGN) with $\mathcal{CN}(0, N_0)$
ν_i	The target rates corresponding for user D_i
$I_\nu(x)$	The modified Besel function of the first class with order ν
$\Gamma(.,.)$	The upper incomplete gamma function
$\Gamma(.)$	The complete gamma function
$G_{1,1}^{1,1}[.]$	The Meijer's G-function

II. SYSTEM MODEL

In this paper, we consider a RIS-enabled NOMA system wherein the base station (S) serves two users, D_i ($i \in \{1, 2\}$), with the assistance of a RIS. We design a RIS with N reflecting metasurfaces and all remaining nodes are facilitated with single antenna. In this circumstance, we assume that the direct-link transmission does not exist due to the blockage. Then, S transmits the superimposed signal $\sum_{j=1}^{2} \sqrt{P_j} x_j$ to D_i. The main parameters can be shown in Table 2. Therefore, the received signal at D_i can be expressed as

$$y_{D_i} = \sqrt{P_S} \sum_{n=1}^{N} g_n \varepsilon_n h_{ni} \sum_{j=1}^{2} \sqrt{P_j} x_j + n_i, \tag{1}$$

where $\varepsilon_n = \varpi_n(\phi_n) e^{j\phi_n}$ is the reflection coefficient produced by the n-th reflector of the RIS, $\varpi_n(\phi_n) = 1$ is the ideal phase shifts ($n = 1, 2, \ldots, N$), g_n and h_{ni} are the channel gain. Moreover, we have $g_n = \frac{f_n e^{-j\theta_n}}{d_{SR}^{\alpha/2}}$, $h_{ni} = \frac{k_{ni} e^{-j\varphi_n}}{\sqrt{d_i^\alpha}}$. According to the result reported in [41], we assume that RIS has perfect knowledge of θ_n and φ_n. Then, the signal to interference plus

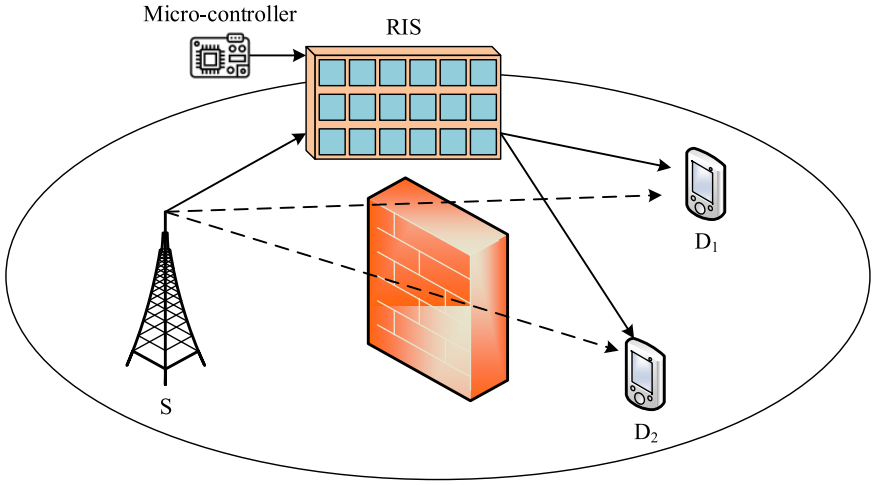

FIGURE 1. System model of the NOMA-RIS system.

noise ratio (SINR) is decode x_2 at D_1 is given by

$$\gamma_{D_1}^{x_2} = \frac{P_S P_2 \left| \sum_{n=1}^{N} f_n k_{n1} e^{j(\phi_n - \theta_n - \varphi_n)} \right|^2}{P_S P_1 \left| \sum_{n=1}^{N} f_n k_{n1} e^{j(\phi_n - \theta_n - \varphi_n)} \right|^2 + d_{SR}^{\alpha} d_1^{\alpha} N_0}. \quad (2)$$

As per the result given [42], we can obtain the maximal SINR by setting $\phi_n = \theta_n + \varphi_n$. [2] Then, we can rewrite (2) as

$$\gamma_{D_1}^{x_2} = \frac{P_S P_2 \left(\sum_{n=1}^{N} f_n k_{n1} \right)^2}{P_S P_1 \left(\sum_{n=1}^{N} f_n k_{n1} \right)^2 + d_{SR}^{\alpha} d_1^{\alpha} N_0}. \quad (3)$$

Moreover, (3) can be simplified as

$$\gamma_{D_1}^{x_2} = \frac{\bar{\gamma}_{D_1} P_2 C_1^2}{\bar{\gamma}_{D_i} P_1 C_1^2 + 1}, \quad (4)$$

where $\eta = \frac{P_S}{N_0}$ denotes the average SNR at the base station, $C_i = \sum_{n=1}^{N} f_n k_{ni}$ and $\bar{\gamma}_{D_i} = \frac{\eta}{d_{SR}^{\alpha} d_i^{\alpha}}$. Then, by employing SIC procedure, the SINR at D_1 used to decode the own signal x_1 is given as

$$\gamma_{D_1}^{x_1} = \bar{\gamma}_{D_1} P_1 C_1^2. \quad (5)$$

Furthermore, the SINR at D_2 used to decode x_2 is computed by

$$\gamma_{D_2}^{x_2} = \frac{\bar{\gamma}_{D_2} P_2 C_2^2}{\bar{\gamma}_{D_2} P_1 C_2^2 + 1}. \quad (6)$$

In the next sections, we examine the system's performance for several scenarios under investigation. These expected results are enough to provide guidelines for implementation of RIS in practical environment.

[2] Although the practical phase shift approach can be considered, we limit our study by ignoring the effect of nonlinear dependency between phase shift and reflection amplitude on the system performance. In particular, we consider the ideal phase shift approach for simplicity. In this regard, the magnitude of reflection factor at each meta-surface is independent of its phase shift, which was widely implemented in [34]–[36].

III. SCHEME I: NOMA-RIS SYSTEM WITHOUT THE DIRECT LINK

A. OUTAGE PERFORMANCE

In this section, the formulas of outage probability for each NOMA destination, D_1 and D_2, are derived. To provide sevices with different QoS requirement, the outage events depend partly on the SNR thresholds relative to the target quality of service of each user.

1) CHANNEL DISTRIBUTION

First, let's denote $C = C_1 = C_2$ and the probability density function (PDF) of C is given as [46]

$$f_{C^2}(\gamma) = \frac{e^{-\frac{\gamma+\lambda}{2\sigma^2}}}{2\sigma^2} \left(\frac{\gamma}{\lambda} \right)^{\frac{-1}{4}} I_{-\frac{1}{2}} \left(\frac{\sqrt{\gamma\lambda}}{\sigma^2} \right), \quad (7)$$

where $\lambda = \left(\frac{N\pi}{4}\right)^2$, $\sigma^2 = N\left(1 - \frac{\pi^2}{16}\right)$ and $I_v(x)$ denotes the modified Bessel function of the first class with order v.

2) OUTAGE PROBABILITY OF D_1

An outage event occurs at user D_1 when its instantaneous received SINR, given as in (5), falls below the threshold SINR γ_1. Consequently, the outage probability of D_1 can be given as

$$OP_{D_1}^{I} = \Pr\left(\gamma_{D_1}^{x_1} < \gamma_1 \right), \quad (8)$$

where $\gamma_i = 2^{v_i} - 1$. Then, with the help of (5), it can be rewritten as

$$\begin{aligned} OP_{D_1}^{I} &= 1 - \Pr\left(C_1^2 > \frac{\gamma_1}{\bar{\gamma}_{D_1} P_1} \right) \\ &= 1 - \int_{\frac{\gamma_1}{\bar{\gamma}_{D_1} P_1}}^{\infty} f_{C_1^2}(x)\, dx. \end{aligned} \quad (9)$$

Then, by the use of (7), we can express (9) as

$$OP_{D_1}^{I} = 1 - \frac{e^{-\frac{\lambda}{2\sigma^2}}}{2\sigma^2\lambda^{-\frac{1}{4}}} \int\limits_{\frac{\gamma_1}{\bar{\gamma}_{D_1}P_1}}^{\infty} x^{\frac{-1}{4}} e^{-\frac{x}{2\sigma^2}} I_{-\frac{1}{2}}\left(\frac{\sqrt{x\lambda}}{\sigma^2}\right) dx. \tag{10}$$

By using the fact that [48, Eq.8.445], $I_v(z) = \sum_{k=0}^{\infty} \frac{1}{k!\Gamma(v+k+1)} \left(\frac{z}{2}\right)^{v+2k}$, we can express the outage probability of D_1 as

$$OP_{D_1}^{I} = 1 - \sum_{k=0}^{\infty} \frac{e^{-\frac{\lambda}{2\sigma^2}}\lambda^k}{k!\Gamma\left(k+\frac{1}{2}\right)} \left(\frac{1}{2\sigma^2}\right)^{\frac{1}{2}+2k} \times \int\limits_{\frac{\gamma_1}{\bar{\gamma}_{D_1}P_1}}^{\infty} x^{k-\frac{1}{2}} e^{-\frac{x}{2\sigma^2}} dx. \tag{11}$$

Finally, using [48, Eq.3.381.3], $OP_{D_1}^{I}$ can be evaluated as

$$OP_{D_1}^{I} = 1 - \sum_{k=0}^{\infty} \frac{e^{-\frac{\lambda}{2\sigma^2}}}{k!\Gamma\left(k+\frac{1}{2}\right)} \left(\frac{\lambda}{2\sigma^2}\right)^{k} \times \Gamma\left(k+\frac{1}{2}, \frac{\gamma_1}{2\sigma^2\bar{\gamma}_{D_1}P_1}\right). \tag{12}$$

3) OUTAGE PROBABILITY OF D_2

We can express the outage probability of D_2 as

$$\begin{aligned} OP_{D_2}^{I} &= \Pr\left(\min\left(\gamma_{D_1}^{x_2}, \gamma_{D_2}^{x_2}\right) > \gamma_2\right) \\ &= 1 - \Pr\left(\gamma_{D_1}^{x_2} < \gamma_2\right) \Pr\left(\gamma_{D_2}^{x_2} > \gamma_2\right). \end{aligned} \tag{13}$$

Then, the closed-form outage probability of D_2 can be obtained as

$$OP_{D_2}^{I} = 1 - P_{out,1} \times P_{out,2}, \tag{14}$$

where $P_{out,1}$ can be expressed as

$$P_{out,1} = \Pr\left(C_1^2 > \frac{\gamma_2}{\bar{\gamma}_{D_1}\vartheta}\right), \tag{15}$$

where $\vartheta = P_2 - \gamma_2 P_1$. Next, it can be calculated as

$$P_{out,1} = \int\limits_{\frac{\gamma_2}{\bar{\gamma}_{D_1}\vartheta}}^{\infty} f_{C_1^2}(x) dx. \tag{16}$$

With the help (7), we can obtain $P_{out,1}$ as

$$P_{out,1} = \sum_{k=0}^{\infty} \frac{e^{-\frac{\lambda}{2\sigma^2}}}{k!\Gamma\left(k+\frac{1}{2}\right)} \left(\frac{\lambda}{2\sigma^2}\right)^{k} \times \Gamma\left(k+\frac{1}{2}, \frac{\gamma_2}{2\sigma^2\bar{\gamma}_{D_1}\vartheta}\right). \tag{17}$$

Similarly, $P_{out,2}$ can be expressed as

$$P_{out,2} = \sum_{k=0}^{\infty} \frac{e^{-\frac{\lambda}{2\sigma^2}}}{k!\Gamma\left(k+\frac{1}{2}\right)} \left(\frac{\lambda}{2\sigma^2}\right)^{k} \times \Gamma\left(k+\frac{1}{2}, \frac{\gamma_2}{2\sigma^2\bar{\gamma}_{D_2}\vartheta}\right). \tag{18}$$

Remark 1: Firstly, due to main results reported in (12), (18) *contain* $\bar{\gamma}_{D_1}$, $\bar{\gamma}_{D_2}$ *which depend on* η, *such outage probabilities depend on the average SNR at the base station* η. *We expect to look the trends of outage probability as varying value of* η *in the section of numerical simulation. Further, the closed-form expressions of outage probability derived in* (12), (18) *point out that they are an increasing function with respect to the number of meta-surface* N *at high SNR regime. Such finding is important result to improve performance of cell-edge users in cellular network since RIS provide higher gain of order* N. *It can be explained that the RIS can attain the inherent aperture gain of order* N *by collecting more signal power.*

Based on explicit results from computations of outage probability, another metric should be considered, i.e., average capacity. We expect to compare system performance of two NOMA users under the context of RIS deployment. We first examine closed-form expressions of average capacity in the next section below.

B. AVERAGE CHANNEL CAPACITY

This section presents the analytical framework that quantifies the average capacity of NOMA-RIS systems, which to the best of authors' knowledge is yet to be studied in the literature. In this sense, we initially present novel a expression for cumulative distribution function (CDF), $F_{\gamma_{D_1}^{x_1}}$, which is computed based on the end-to-end SINR of the NOMA-RIS system. By this regard, $F_{\gamma_{D_1}^{x_1}}$ is PDF which need be examined. To this end, we try to find the closed-form formulas of the average capacity which can be applied to the two cases, i.e. NOMA system with and without RIS.

The average channel capacity of D_1 can be evaluated as

$$R_{D_1}^{I} = \frac{1}{\ln(2)} \int_0^{\infty} \frac{1 - F_{\gamma_{D_1}^{x_1}}(x)}{(1+x)} dx. \tag{19}$$

Proposition 1: The closed-form expression of average capacity $R_{D_1}^{I}$ can be expressed as

$$R_{D_1}^{I} = \frac{1}{\ln(2)} \sum_{k=0}^{\infty} \frac{e^{-\frac{\lambda}{2\sigma^2}}}{k!\Gamma\left(k+\frac{1}{2}\right)} \left(\frac{\lambda}{2\sigma^2}\right)^{k} \times G_{2,3}^{3,1}\left[\begin{matrix} 0, 1 \\ 0, k+\frac{1}{2}, 0 \end{matrix} \middle| \frac{1}{2\bar{\gamma}_{D_1}P_1\sigma^2}\right]. \tag{20}$$

Proof: See Appendix for the detailed analysis.

The average channel capacity of D_2 is given as

$$R_{D_2}^{I} = \frac{1}{\ln(2)} \int_0^{P_2/P_1} \frac{1 - F_{\gamma_{D_2}^{x_2}}(x)}{(1+x)} dx. \tag{21}$$

Proposition 2: The closed-form expression to point out average capacity of user D_2, i.e.n $R^I_{D_2}$ is expressed by

$$R^I_{D_2} \approx \frac{1}{\ln(2)} \sum_{k=0}^{\infty} \frac{e^{-\frac{\lambda}{2\sigma^2}}}{k!\Gamma\left(k+\frac{1}{2}\right)} \left(\frac{\lambda}{2\sigma^2}\right)^k \times \sum_{m=1}^{M} \frac{\pi\sqrt{1-\zeta_m^2}}{M\left(\frac{2P_1}{P_2}+\zeta_m+1\right)} \Gamma \times \left(k+\frac{1}{2}, \frac{(\zeta_m+1)}{2\sigma^2\bar{\gamma}_{D_2}P_1(1-\zeta_m)}\right). \quad (22)$$

Proof: The CDF of $\gamma^{x_2}_{D_2}$ can be expressed by

$$F_{\gamma^{x_2}_{D_2}} = 1 - \sum_{k=0}^{\infty} \frac{e^{-\frac{\lambda}{2\sigma^2}}}{k!\Gamma\left(k+\frac{1}{2}\right)} \left(\frac{\lambda}{2\sigma^2}\right)^k \times \Gamma\left(k+\frac{1}{2}, \frac{x}{2\sigma^2\bar{\gamma}_{D_2}(P_2-xP_1)}\right). \quad (23)$$

Substituting (23) into (21), we have

$$R^I_{D_2} = \frac{1}{\ln(2)} \sum_{k=0}^{\infty} \frac{e^{-\frac{\lambda}{2\sigma^2}}}{k!\Gamma\left(k+\frac{1}{2}\right)} \left(\frac{\lambda}{2\sigma^2}\right)^k \times \int_0^{P_2/P_1} \frac{\Gamma\left(k+\frac{1}{2}, \frac{x}{2\sigma^2\bar{\gamma}_{D_2}(P_2-xP_1)}\right)}{(1+x)} dx. \quad (24)$$

Now, using Gaussian-Chebyshev property with $\zeta_m = \cos\left(\frac{2m-1}{2M}\pi\right)$ and solving the integral, we can obtain (22).

This completes the proof.

Remark 2: Since main results reported in (20), (22) *contain common term which depends on the number of meta-surface N, we expect that the average capacity performance relies mainly on values of N. Therefore, it is likely important to enhance capacity performance by increasing meta-surface in the RIS. However, two users exhibit different SINRs, and hence performance gap among two users exist once we increase η to look how the average performance of two user can improve. This finding lead to further confirmation by comparing RIS system with traditional relaying system.*

IV. THE BENCHMARK–SCHEME II: RELAY SYSTEM

In this scheme, we replace a RIS by a normal relay (denoted as R).[3] For the relaying system with the Decode-and-Forward (DF) protocol, the SINR of R when detected x_1 and x_2 in the first phase are given, respectively, as [27], [28]

$$\gamma^{II}_{R,x_2} = \frac{\eta P_2 |g|^2}{\eta P_1 |g|^2 + d^{\alpha}_{SR}}, \quad (25)$$

and

$$\gamma^{II}_{R,x_1} = \frac{\eta P_1 |g|^2}{d^{\alpha}_{SR}}. \quad (26)$$

In the second phase, the SINR at D_1 when detected x_2 and then the SINR achieved by employing SIC to detect x_1 are given, respectively, as

$$\gamma^{II}_{D_1,x_2} = \frac{\eta P_2 |h_1|^2}{\eta P_1 |h_1|^2 + d^{\alpha}_1}, \quad (27)$$

and

$$\gamma^{II}_{D_1,x_1} = \frac{\eta P_1 |h_1|^2}{d^{\alpha}_1}. \quad (28)$$

Moreover, the SINR at D_2 to detect x_2 is given as

$$\gamma^{II}_{D_2,x_2} = \frac{\eta P_2 |h_1|^2}{\eta P_1 |h_1|^2 + d^{\alpha}_1}. \quad (29)$$

A. OUTAGE PERFORMANCE

The outage probability of D_i can be given as

$$OP^{II}_{D_i} = \Pr\left(\min\left(\gamma^{II}_{R,x_i}, \gamma^{II}_{D_i,x_i}\right) < \gamma^{II}_i\right), \quad (30)$$

where $\gamma^{II}_i = 2^{2v_i} - 1$. The closed-form expression of the outage probability for user D_1 is calculated as

$$\begin{aligned} OP^{II}_{D_1} &= \Pr\left(\min\left(\gamma^{II}_{R,x_1}, \gamma^{II}_{D_1,x_1}\right) < \gamma^{II}_1\right) \\ &= 1 - \Pr\left(|g|^2 > \frac{\gamma^{II}_1 d^{\alpha}_{SR}}{\eta P_1}, |h_1|^2 > \frac{\gamma^{II}_1 d^{\alpha}_1}{\eta P_1}\right) \\ &= 1 - e^{-\frac{\gamma^{II}_1 d^{\alpha}_{SR}}{\eta P_1}} e^{-\frac{\gamma^{II}_1 d^{\alpha}_1}{\eta P_1}}. \end{aligned} \quad (31)$$

Similarly, the closed-form expression of the outage probability for user D_2 can be obtained as

$$OP^{II}_{D_2} = 1 - e^{-\frac{\gamma^{II}_2 d^{\alpha}_{SR}}{\eta\left(P_2 - \gamma^{II}_2 P_1\right)}} e^{-\frac{\gamma^{II}_2 d^{\alpha}_2}{\eta\left(P_2 - \gamma^{II}_2 P_1\right)}}. \quad (32)$$

B. AVERAGE CHANNEL CAPACITY

expression of the average channel capacity of D_1 by

$$R^{II}_{D_1} = \frac{1}{2\ln(2)} \int_0^{\infty} \frac{1 - F_{Z_1}(x)}{1+x} dx, \quad (33)$$

where $Z_i = \min\left(\gamma^{II}_{R,x_i}, \gamma^{II}_{D_i,x_i}\right)$. Then, with the help of [48, Eq. (3.352.4)] we can express (33) as

$$\begin{aligned} R^{II}_{D_1} &= \frac{1}{2\ln(2)} \int_0^{\infty} \frac{e^{-\frac{d^{\alpha}_{SR}+d^{\alpha}_1}{\eta P_1}x}}{1+x} dx \\ &= \frac{-1}{2\ln(2)} e^{\frac{d^{\alpha}_{SR}+d^{\alpha}_1}{\eta P_1}} Ei\left(-\frac{d^{\alpha}_{SR}+d^{\alpha}_1}{\eta P_1}\right). \end{aligned} \quad (34)$$

[3]The total power dissipated to operate the considered NOMA-RIS system or NOMA relaying system is composed of the base station transmit power, the hardware static power consumed in the base station, mobile users, and RIS or relay. Since RIS's reflectors are passive elements that do not directly alter the magnitude of the incoming signal, the RIS does not require any transmit power. However, RIS provides amplification gain by achieving a suitable adjustment of the phase shifts of the reflecting elements with a phase coherence. In contrast, a relay need separated power for its operation. As a result, NOMA relaying system has significant difference compared to NOMA-RIS architectures, which points out the important benefit of RIS.

Next, the average channel capacity of D_2 is expressed as

$$R_{D_2}^{II} = \frac{1}{2\ln(2)} \int_0^{P_2/P_1} \frac{1 - F_{Z_2}(x)}{1+x} dx. \tag{35}$$

Similarly, the closed-form expression of (35) can be obtained as

$$R_{D_1}^{II} \approx \frac{1}{2\ln(2)} \sum_{m=1}^{M} \frac{\pi\sqrt{1-\zeta_m^2}}{M\left(\frac{2P_1}{P_2}+\zeta_m+1\right)} e^{-\frac{\left(d_{SR}^{\alpha}+d_2^{\alpha}\right)(1+\zeta_m)}{\eta P_1(1-\zeta_m)}}. \tag{36}$$

V. SCHEME III: NOMA-RIS SYSTEM WITH THE DIRECT LINK

For the scenario, when the direct links between S and D_i are present, the received signal at D_i is given as

$$y_{D_i}^{III} = \sqrt{P_S}\left(h_{SD_i} + \sum_{n=1}^{N} g_n \varepsilon_n h_{ni}\right) \times \sum_{j=1}^{2} \sqrt{P_j} x_j + n_i, \tag{37}$$

where $h_{SD_i} = \frac{f_{SD_i}}{d_{SD_i}^{\alpha/2}}$. Then, the SINR to decode x_2 at D_1 is given by

$$\gamma_{D_1,x_2}^{III} = \frac{P_S P_2 \left(\frac{|f_{SD_1}|}{d_{SD_1}^{\alpha/2}} + \frac{\left|\sum_{n=1}^{N} f_n k_{n1}\right|}{(d_{SR} d_1)^{\alpha/2}}\right)^2}{P_S P_1 \left(\frac{|f_{SD_1}|}{d_{SD_1}^{\alpha/2}} + \frac{\left|\sum_{n=1}^{N} f_n k_{n1}\right|}{(d_{SR} d_1)^{\alpha/2}}\right)^2 + N_0}. \tag{38}$$

To simpler manipulation, (38) can be rewritten as

$$\gamma_{D_1,x_2}^{III} = \frac{\eta P_2 U_1}{\eta P_1 U_1 + 1}, \tag{39}$$

where $U_i = \left(\frac{|f_{SD_1}|}{d_{SD_1}^{\alpha/2}} + \frac{\left|\sum_{n=1}^{N} f_n k_{n1}\right|}{(d_{SR} d_1)^{\alpha/2}}\right)^2$.

Next, the SINR at D_1 used to decode its own signal x_1 is formulated by

$$\gamma_{D_1,x_1}^{III} = \eta P_1 U_1, \tag{40}$$

Considering signal at D_2, the SINR used to decode x_2 is expressed as

$$\gamma_{D_2,x_2}^{III} = \frac{\eta P_2 U_2}{\eta P_1 U_2 + 1}. \tag{41}$$

We continue to examine the system performance metrics as the next subsections.

A. OUTAGE PERFORMANCE

1) CHANNEL STATISTICS

By employing results reported in [43], the CDF of U_i can be obtained as

$$F_{U_i}(x) = 1 - \Gamma\left(a_i, \frac{\sqrt{x}}{b_i}\right) / \Gamma(a_i), \tag{42}$$

where a and b are calculated by

$$a_i = \frac{\left(\sqrt{d_{SD_i}^{-\alpha/2}\pi} + 2N\tilde{a}\tilde{b}_i\right)}{4 + d_{SD_i}^{-\alpha/2} + 4N\tilde{a}\tilde{b}_i^2 - d_{SD_i}^{-\alpha/2}\pi}, \tag{43}$$

$$b_i = \frac{4d_{SD_i}^{-\alpha/2} + 4N\tilde{a}\tilde{b}_i^2 - d_{SD_i}^{-\alpha/2}\pi}{2\left(\sqrt{d_{SD_i}^{-\alpha/2}\pi} + 2N\tilde{a}\tilde{b}_i\right)}, \tag{44}$$

in which $\tilde{a} = \frac{\pi^2}{(16-\pi^2)}$ and $\tilde{b}_i = \left(4 - \frac{\pi^2}{4}\right)\frac{\sqrt{(d_{SR}d_i)^{-\alpha/2}}}{\pi}$.

2) OUTAGE PROBABILITY OF D_1

The outage probability of D_1 can be computed as

$$\begin{aligned} OP_{D_1}^{III} &= \Pr\left(\gamma_{D_1,x_1}^{III} < \gamma_1\right) \\ &= 1 - \Pr\left(U_1 > \frac{\gamma_1}{\eta P_1}\right) \\ &= 1 - \Gamma\left(a_1, \sqrt{\frac{\gamma_1}{\eta P_1 b_1^2}}\right) / \Gamma(a_1) \end{aligned} \tag{45}$$

Then, the outage probability of D_2 can be expressed as

$$\begin{aligned} OP_{D_2}^{III} &= \Pr\left(\min\left(\gamma_{D_1,x_2}^{III}, \gamma_{D_2,x_2}^{III}\right) < \gamma_2\right) \\ &= 1 - \bar{P}_{out,1} \times \bar{P}_{out,2}. \end{aligned} \tag{46}$$

As further steps, $P_{out,1}$ is given as

$$\begin{aligned} \bar{P}_{out,1} &= \Pr\left(\gamma_{D_1}^{x_2} > \gamma_2\right) = \Pr\left(U_1 > \frac{\gamma_2}{\eta\vartheta}\right) \\ &= \frac{\Gamma\left(a_1, \sqrt{\frac{\gamma_2}{\eta\vartheta b_1^2}}\right)}{\Gamma(a_1)}. \end{aligned} \tag{47}$$

Similarly, $P_{out,2}$ can be formulated as

$$\begin{aligned} \bar{P}_{out,2} &= \Pr\left(\gamma_{D_2}^{x_2} > \gamma_2\right) = \Pr\left(U_2 > \frac{\gamma_2}{\eta\vartheta}\right) \\ &= \frac{\Gamma\left(a_2, \sqrt{\frac{\gamma_2}{\eta\vartheta b_2^2}}\right)}{\Gamma(a_2)}. \end{aligned} \tag{48}$$

VI. NUMERICAL RESULTS

In this section, we evaluate several scenarios with a set of the parameters, shown in Table 3, which are similar to [4], [45], except for some specific cases. In the following figures, Monte-Carlo simulations are performed to validate the analytical results. In these figures, we denote "Simulation" for the simulated curves relying on Monte-carlo and "Analytical" for analytical ones obtained with the expressions derived in the previous sections.

TABLE 3. Table of Parameters.

The reflecting meta-surfaces	$N = 5$
Power allocation coefficients	$P_1 = 0.2$ and $P_2 = 0.8$
The pass-loss exponent	$\alpha = 2$
The target rates	$\nu_1 = \nu_2 = 1$ bit per channel use (BPCU)
The distances from S to RIS	$d_{SR} = 5m$
The distances from RIS to D_i	$d_1 = 5m$ and $d_2 = 10m$
The distances from S to D_i	$d_{SD_1} = 5m$ and $d_{SD_2} = 10m$

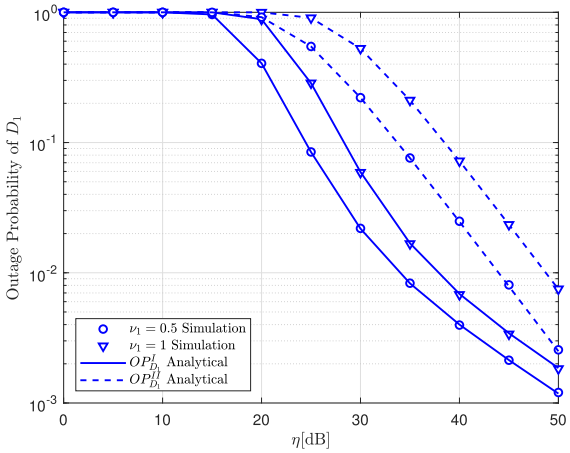

FIGURE 2. Outage probability of D_1 versus η in two schemes with different target rates ν_1.

Fig. 2 compares the outage probability versus the transmit SNR at the base station for two schemes by considering target rate as $\nu_1 = 0.5$ and $\nu_1 = 1$. By increasing transmit SNR η, one can achieve better outage performance, especially such outage behavior can be improved significantly at very high SNR regime, i.e. when $\eta = 50$ (dB), the outage probability of the first user in NOMA-RIS system is around 10^{-3}. It can be clearly seen that SINRs to detect signal for both users depend on the thresholds, while such threshold is decided by $\nu_1 = 0.5$. As a result, higher requirement of target rate leads to worse outage performance. Obviously, by achieving advances of RIS, NOMA-RIS exhibits better performance compare with NOMA scheme using relay. Performance gap can be observed clearly when we compare performance of NOMA with and without RIS once η belongs to the range from 20 (dB) to 45 (dB). Besides, the Monte-Carlo based simulation results are matched very well with the analytical results, which confirms the exactness of our derived expressions.

We make another comparison of the outage probability performance when adopting the considered NOMA-RIS with the varying number of RIS reflecting elements N, as shown in Fig. 3. The higher value of N leads to significant improvement in term of outage probability performance at high SNR region. For example, the outage performance in the NOMA-RIS system can be reduced significantly for $N = 20$. When the number of reflecting elements N increases, this advantage of RIS to the NOMA-RIS system is further

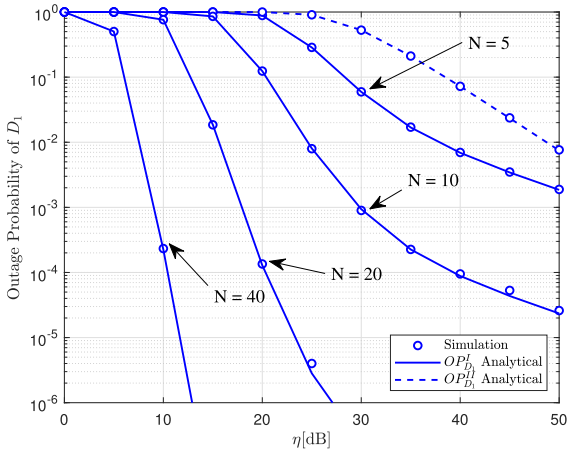

FIGURE 3. Outage probability of D_1 versus η in two schemee with different metasuface of RIS N.

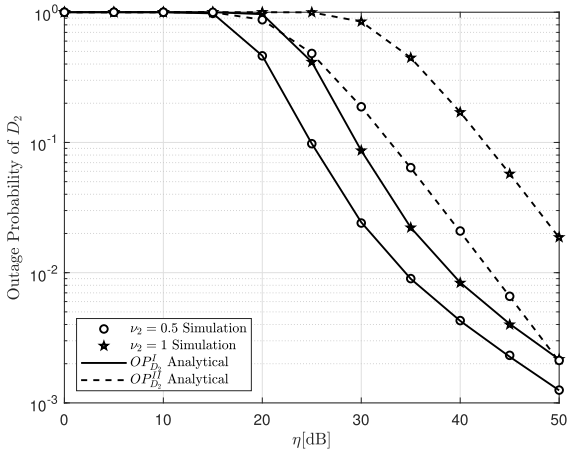

FIGURE 4. Outage probability of D_2 versus η in two schemes with different target rates ν_2.

enlarged. In addition, with the increase of N from 20 to 40, the advantages of the NOMA-RIS system are more significant.

Similarly, the outage probability of the second user D_2 also reduces at high SNR as presented in Fig. 4. For instance, at an average transmit SNR of 50 dB, the outage probability for the case of $\nu_2 = 0.5$ equals to 10^{-3}. When we compare two cases of target rate ν_2, the performance gap at NOMA-RIS is smaller than that of NOMA relying on relay. Although decoding procedures and conditions for computing outage probability at user D_2 is different compared to user D_1, but the similar trends of such outage behavior can be seen in Fig. 2, Fig. 3 and Fig. 4. This is because the expressions of outage probability depend mainly on the transmit SNR η, and hence same trends are concluded for both users.

As can be seen from Fig. 5, the number of reflecting meta-surface N contributes to improvement of outage probability for the second user, similar case as seen in Fig. 3. Since main equations of outage probability contain SINRs represented in (2), (4) and (6) which then contain

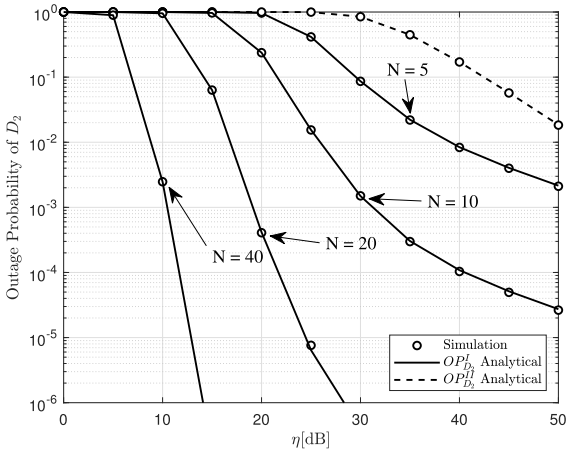

FIGURE 5. Outage probability of D_2 versus η in two schemes with different metasurfaces N.

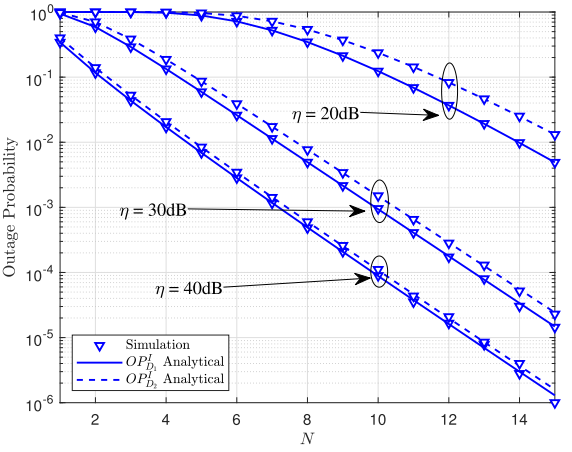

FIGURE 7. Outage probability versus N in Scheme I with different transmit SNR at the BS η.

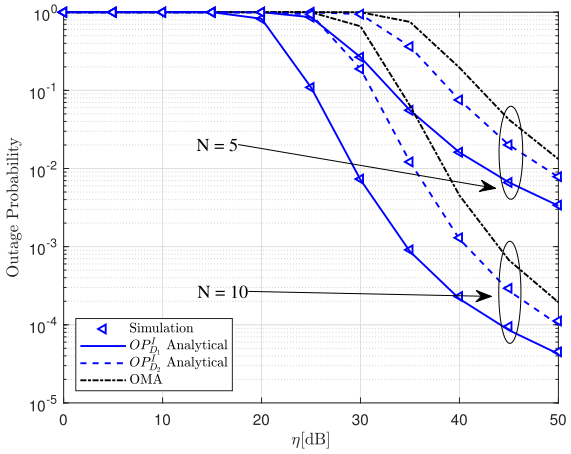

FIGURE 6. Outage probability versus η in Scheme I with different metasurfaces N, where $v_1 = v_2 = 2$ (BPCU).

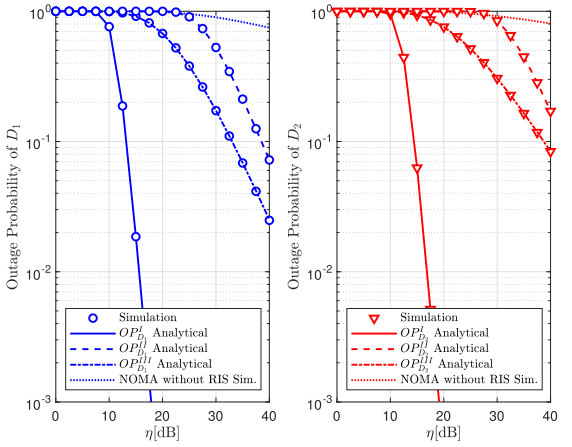

FIGURE 8. Comparison of outage probabilities versus η in 3 schemes where $N = 20$.

channel coefficients improved by increasing number of meta-surface N, and hence the outage probability would be better at higher value of N.

To compare outage performance of two users under the impact of the number of meta-surface N, Fig. 6 demonstrates the outage probability versus the transmit SNR for the NOMA-RIS and orthogonal multiple access (OMA) enabled RIS systems. It is seen clearly that RIS system relying NOMA scheme shows better outage probability compared with RIS using OMA. As can be seen from Fig. 6, the second user D_2 exhibits its superiority compared with that of user D_1 in terms of outage performance. It can be explained that different power coefficients P_1, P_2 allocated two users make influence to expressions of SINRs, and then the corresponding outage probability. In addition, conditions of decoding signals at two users are different, and hence values of outage probability of two users are dissimilar. In cases of $\eta = 40dB$ and $N = 10$, $OP^I_{D1} = 0.0002$, $OP^I_{D2} = 0.0012$ and OMA equal 0.004. When we compare our study with OMA, the improvement of OP^I_{D1} and OP^I_{D2} are respectively 0.38% and 0.28%.

In Fig. 7, by increasing the number of metasurfaces N from 2 to 14, the outage behavior can be improved significantly, especially for two cases, $\eta = 30dB$, and $\eta = 40dB$. The performance gap among two users is very small for case of $\eta = 40dB$ regardless of any values of N. It can be explained by intelligent adjustment of phase shifts by enabling RIS, so that the SINRs at destinations can be maximized, and hence the outage probability can be improved. Therefore, the role of RIS design is crucial to the main task of enhancing performance at destinations.

To extend our consideration on outage performance, we compare three schemes in Fig. 8. The main finding in Fig. 8 indicates that the considered systems facilitated with RIS provide better performance compared with traditional relaying system. It is strict confirmation the meaningful deployment of RIS in such system. In addition, when $\eta = 20dB$, $OP^I_{D1} = 0.0001$, $OP^{II}_{D1} = 0.9994$ and $OP^{III}_{D1} = 0.6749$ and without RIS equal 0.986. The improvement of OP^I_{D1} with OP^{II}_{D1}, OP^{III}_{D1} and without RIS in outage probability are

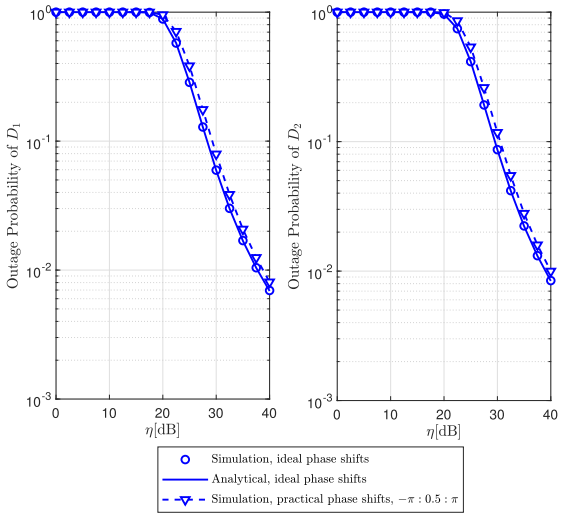

FIGURE 9. Considering phase shift for outage probability performance, $v_1 = v_2 = 1$ (BPCU) and $N = 5$.

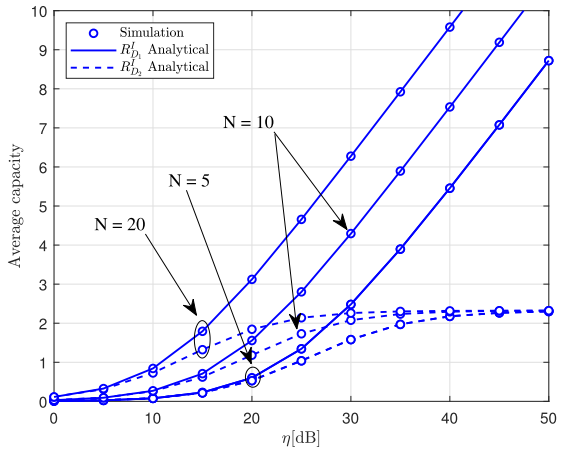

FIGURE 10. The average capacity versus η with different N.

99.93%, 67.48% and 98.65%. Similarly, we can easy obtain the improvement of D_2 in Scheme I.

In Fig. 9, we consider how imperfect phase shift make influence to RIS-aided systems at two destinations D_1 and D_2. It can be intuitively seen that the performance loss might occur since the ideal and practical phase shifts are emphasized as factor affecting the outage performance. From [44], the practical phase shifts lead to the performance loss by considering $\varpi_n(\varphi_n) = (1 - \omega_{\min})\left(\frac{\sin(\varphi_n - \kappa)+1}{2}\right)^{\varsigma} + \omega_{\min}$, where $\omega_{\min}$ represents for the minimum amplitude, κ is denoted as the horizontal distance between $\frac{\pi}{2}$ and $\omega_{\min}$, ς is the steepness of function curve. In this circumstance, our setup parameters are $\omega_{\min} = 0.8$, $\kappa = 0.43\pi$ and $\varsigma = 1.6$. It can be concluded that a certain performance loss will be raised when we compare the considered system relying on the practical and ideal phase shifts.

In view of the average capacity performance in Fig. 10, the superiority of the first user D_1 over the second user D_2 becomes more significant as η increases. This is because of the reason that (5) mainly depends on η, and hence the average capacity. Similar trends as outage probability presented in Fig. 2-Fig. 6, the average capacity has main affection from the number of meta-surface N. In three cases of N, the average capacity values of user D_2 are same when we consider them at the point η is greater than 45 (dB). We can explain that average rates depend on SINRs, while (5), (6) are SINRs which indicate difference for detecting signals x_1, x_2, respectively. In (5), SINR is linear increase of C_1 which relies on SNR η, while SINR in (6) contains C_2 in both numerator and denominator, and hence average rate is limited at high η region. In the contrast, considering performance among three cases of N, the average capacity values of user D_1 show larger gaps.

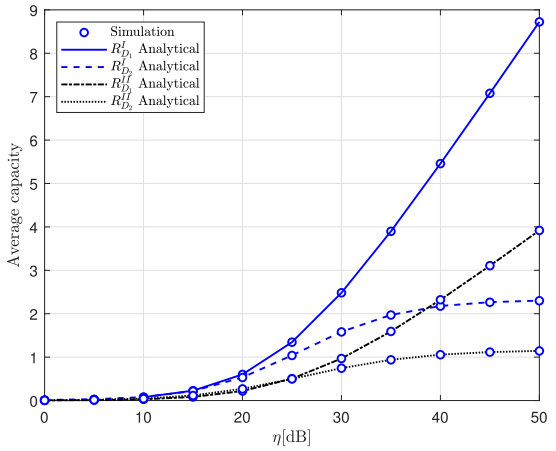

FIGURE 11. Comparison of average capacity in Scheme I and Scheme II versus η.

It is worth noting that NOMA-RIS shows its advantage once we compare it with NOMA using traditional relay, shown in Fig. 11. The superiority of the NOMA-RIS can be concluded for two users, which shows the impact of architecture of RIS to improve the average capacity at both users. As a result, the proposed protocol outperforms the NOMA with relaying in terms of outage probability and average capacity. It is worth noting that the NOMA-RIS shows significant improvement when transmit SNR η is greater 40 (dB).

VII. CONCLUSION

In this paper, the benefits of joint NOMA and RIS techniques have been investigated. The base station enables fixed power allocation scheme to send superimposed signals to serve a dedicated group of two users. It shows significant benefit when we adopt RIS and hence the improvement can be shown by comparing NOMA system with and without RIS. Especially, we consider various practical circumstances, such as, direct link, system without RIS, imperfect phase shifts. For such setup, we derived the analytical closed-form formulas of the outage probability and average capacity, which are useful to understand how the system/channel parameters affecting to the system's performance. The main results showed that

the NOMA RIS outperforms OMA RIS, which explicitly confirms advances of RIS in terms of outage performance and average capacity. Our analytical and simulation results reveal that the higher number of the reflective elements at the RIS can be intelligently controlled to boost the outage probability and average capacity significantly at high SNR regime.

APPENDIX

To compute the closed-form expression of average capacity, we first calculate the CDF of $\gamma_{D_1}^{x_1}$, and it can be obtained as

$$F_{\gamma_{D_1}^{x_1}}(x) = 1 - \sum_{k=0}^{\infty} \frac{e^{-\frac{\lambda}{2\sigma^2}}}{k!\Gamma\left(k+\frac{1}{2}\right)} \left(\frac{\lambda}{2\sigma^2}\right)^k \times \Gamma\left(k+\frac{1}{2}, \frac{x}{2\bar{\gamma}_{D_1} P_1 \sigma^2}\right). \quad (49)$$

Substituting (49) into (19), we can have

$$R_{D_1}^I = \frac{1}{\ln(2)} \sum_{k=0}^{\infty} \frac{e^{-\frac{\lambda}{2\sigma^2}}}{k!\Gamma\left(k+\frac{1}{2}\right)} \left(\frac{\lambda}{2\sigma^2}\right)^k \times \int_0^{\infty} \frac{\Gamma\left(k+\frac{1}{2}, \frac{x}{2\bar{\gamma}_{D_1} P_1 \sigma^2}\right)}{(1+x)} dx. \quad (50)$$

Using [47, Eq. 5], we can write

$$\Gamma(\alpha, x) = G_{1,2}^{2,0}\left[\begin{matrix} 1 \\ \alpha, 0 \end{matrix} \middle| x\right]. \quad (51)$$

Next, (49) can be calculated as

$$R_{D_1}^I = \frac{1}{\ln(2)} \sum_{k=0}^{\infty} \frac{e^{-\frac{\lambda}{2\sigma^2}}}{k!\Gamma\left(k+\frac{1}{2}\right)} \left(\frac{\lambda}{2\sigma^2}\right)^k \times \int_0^{\infty} \frac{G_{1,2}^{2,0}\left[\begin{matrix} 1 \\ k+\frac{1}{2}, 0 \end{matrix} \middle| \frac{x}{2\bar{\gamma}_{D_1} P_1 \sigma^2}\right]}{(1+x)} dx. \quad (52)$$

Based on [48, Eq. 7.811.5], the closed-form formula of $R_{D_1}^I$ can be obtained as

$$R_{D_1}^I = \frac{1}{\ln(2)} \sum_{k=0}^{\infty} \frac{e^{-\frac{\lambda}{2\sigma^2}}}{k!\Gamma\left(k+\frac{1}{2}\right)} \left(\frac{\lambda}{2\sigma^2}\right)^k \times G_{2,3}^{3,1}\left[\begin{matrix} 0, 1 \\ 0, k+\frac{1}{2}, 0 \end{matrix} \middle| \frac{1}{2\bar{\gamma}_{D_1} P_1 \sigma^2}\right]. \quad (53)$$

This is the end of the proof.

REFERENCES

[1] Q. Wu and R. Zhang, "Intelligent reflecting surface enhanced wireless network via joint active and passive beamforming," *IEEE Trans. Wireless Commun.*, vol. 18, no. 11, pp. 5394–5409, Nov. 2019.

[2] S. Atapattu, R. Fan, P. Dharmawansa, G. Wang, J. Evans, and T. A. Tsiftsis, "Reconfigurable intelligent surface assisted two-way communications: Performance analysis and optimization," *IEEE Trans. Commun.*, vol. 68, no. 10, pp. 6552–6567, Oct. 2020.

[3] L. Yang, F. Meng, Q. Wu, D. B. da Costa, and M.-S. Alouini, "Accurate closed-form approximations to channel distributions of RIS-aided wireless systems," *IEEE Wireless Commun. Lett.*, vol. 9, no. 11, pp. 1985–1989, Nov. 2020.

[4] Z. Ding, R. Schober, and H. V. Poor, "On the impact of phase shifting designs on IRS-NOMA," *IEEE Wireless Commun. Lett.*, vol. 9, no. 10, pp. 1596–1600, Oct. 2020.

[5] A. Hemanth, K. Umamaheswari, A. C. Pogaku, D.-T. Do, and B. M. Lee, "Outage performance analysis of reconfigurable intelligent surfaces-aided NOMA under presence of hardware impairment," *IEEE Access*, vol. 8, pp. 212156–212165, 2020.

[6] M. Hua, Q. Wu, D. Wing Kwan Ng, J. Zhao, and L. Yang, "Intelligent reflecting surface-aided joint processing coordinated multipoint transmission," 2020, *arXiv:2003.13909*. [Online]. Available: http://arxiv.org/abs/2003.13909

[7] C. Pan, H. Ren, K. Wang, W. Xu, M. Elkashlan, A. Nallanathan, and L. Hanzo, "Multicell MIMO communications relying on intelligent reflecting surfaces," *IEEE Trans. Wireless Commun.*, vol. 19, no. 8, pp. 5218–5233, Aug. 2020.

[8] H. Guo, Y.-C. Liang, J. Chen, and E. G. Larsson, "Weighted sum-rate optimization for intelligent reflecting surface enhanced wireless networks," 2019, *arXiv:1905.07920*. [Online]. Available: http://arxiv.org/abs/1905.07920

[9] S. Hu, Z. Wei, Y. Cai, D. Wing Kwan Ng, and J. Yuan, "Sum-rate maximization for multiuser MISO downlink systems with self-sustainable IRS," 2020, *arXiv:2005.11663*. [Online]. Available: http://arxiv.org/abs/2005.11663

[10] M. Hua, Q. Wu, D. Wing Kwan Ng, J. Zhao, and L. Yang, "Intelligent reflecting surface-aided joint processing coordinated multipoint transmission," 2020, *arXiv:2003.13909*. [Online]. Available: http://arxiv.org/abs/2003.13909

[11] Q. Wu and R. Zhang, "Joint active and passive beamforming optimization for intelligent reflecting surface assisted SWIPT under QoS constraints," *IEEE J. Sel. Areas Commun.*, vol. 38, no. 8, pp. 1735–1748, Aug. 2020.

[12] Q. Wu and R. Zhang, "Weighted sum power maximization for intelligent reflecting surface aided SWIPT," *IEEE Wireless Commun. Lett.*, vol. 9, no. 5, pp. 586–590, May 2020.

[13] Y. Yang, B. Zheng, S. Zhang, and R. Zhang, "Intelligent reflecting surface meets OFDM: Protocol design and rate maximization," 2019, *arXiv:1906.09956*. [Online]. Available: http://arxiv.org/abs/1906.09956

[14] B. Zheng, Q. Wu, and R. Zhang, "Intelligent reflecting surface-assisted multiple access with user pairing: NOMA or OMA?" *IEEE Commun. Lett.*, vol. 24, no. 4, pp. 753–757, Apr. 2020.

[15] Y. Li, M. Jiang, Q. Zhang, and J. Qin, "Joint beamforming design in multi-cluster MISO NOMA intelligent reflecting surface-aided downlink communication networks," 2019, *arXiv:1909.06972*. [Online]. Available: http://arxiv.org/abs/1909.06972

[16] X. Guan, Q. Wu, and R. Zhang, "Intelligent reflecting surface assisted secrecy communication: Is artificial noise helpful or not?" *IEEE Wireless Commun. Lett.*, vol. 9, no. 6, pp. 778–782, Jun. 2020.

[17] H. Shen, W. Xu, S. Gong, Z. He, and C. Zhao, "Secrecy rate maximization for intelligent reflecting surface assisted multi-antenna communications," *IEEE Commun. Lett.*, vol. 23, no. 9, pp. 1488–1492, Sep. 2019.

[18] X. Guan, Q. Wu, and R. Zhang, "Joint power control and passive beamforming in irs-assisted spectrum sharing," *IEEE Commun. Lett.*, vol. 24, no. 7, pp. 1153–1157, Jul. 2020.

[19] T. Bai, C. Pan, Y. Deng, M. Elkashlan, A. Nallanathan, and L. Hanzo, "Latency minimization for intelligent reflecting surface aided mobile edge computing," *IEEE J. Sel. Areas Commun.*, vol. 38, no. 11, pp. 2666–2682, Nov. 2020.

[20] X. Li, M. Zhao, M. Zeng, S. Mumtaz, V. G. Menon, Z. Ding, and O. A. Dobre, "Hardware impaired ambient backscatter NOMA systems: Reliability and security," *IEEE Trans. Commun.*, vol. 69, no. 4, pp. 2723–2736, Apr. 2021, doi: 10.1109/TCOMM.2021.3050503.

[21] D.-T. Do, M.-S.-V. Nguyen, F. Jameel, R. Jantti, and I. S. Ansari, "Performance evaluation of relay-aided CR-NOMA for beyond 5G communications," *IEEE Access*, vol. 8, pp. 134838–134855, 2020.

[22] D.-T. Do, T.-L. Nguyen, K. M. Rabie, X. Li, and B. M. Lee, "Throughput analysis of multipair two-way replaying networks with NOMA and imperfect CSI," *IEEE Access*, vol. 8, pp. 128942–128953, 2020.

[23] B. Wang, F. Gao, S. Jin, H. Lin, and G. Y. Li, "Spatial- and frequency-wideband effects in millimeter-wave massive MIMO systems," *IEEE Trans. Signal Process.*, vol. 66, no. 13, pp. 3393–3406, Jul. 2018.

[24] X. Li, M. Zhao, Y. Liu, L. Li, Z. Ding, and A. Nallanathan, "Secrecy analysis of ambient backscatter NOMA systems under I/Q imbalance," *IEEE Trans. Veh. Technol.*, vol. 69, no. 10, pp. 12286–12290, Oct. 2020.
[25] C. Chen, W. Cai, X. Cheng, L. Yang, and Y. Jin, "Low complexity beamforming and user selection schemes for 5G MIMO-NOMA systems," *IEEE J. Sel. Areas Commun.*, vol. 35, no. 12, pp. 2708–2722, Dec. 2017.
[26] S. Baig, U. Ali, H. M. Asif, A. A. Khan, and S. Mumtaz, "Closed-form BER expression for Fourier and wavelet transform-based pulse-shaped data in downlink NOMA," *IEEE Commun. Lett.*, vol. 23, no. 4, pp. 592–595, Apr. 2019.
[27] D.-T. Do, A.-T. Le, C.-B. Le, and B. M. Lee, "On exact outage and throughput performance of cognitive radio based non-orthogonal multiple access networks with and without D2D link," *Sensors*, vol. 19, no. 15, p. 3314, Jul. 2019.
[28] D.-T. Do, A.-T. Le, and B. M. Lee, "NOMA in cooperative underlay cognitive radio networks under imperfect SIC," *IEEE Access*, vol. 8, pp. 86180–86195, 2020.
[29] Y. Li, M. Jiang, Q. Zhang, Q. Li, and J. Qin, "Cooperative non-orthogonal multiple access in multiple-input-multiple-output channels," *IEEE Trans. Wireless Commun.*, vol. 17, no. 3, pp. 2068–2079, Mar. 2018.
[30] T.-L. Nguyen and D.-T. Do, "Power allocation schemes for wireless powered NOMA systems with imperfect CSI: An application in multiple antenna-based relay," *Int. J. Commun. Syst.*, vol. 31, no. 15, p. e3789, Oct. 2018.
[31] Y. Akhmetkaziyev, G. Nauryzbayev, S. Arzykulov, A. M. Eltawil, K. M. Rabie, and X. Li, "Performance of NOMA-enabled cognitive satellite-terrestrial networks with non-ideal system limitations," *IEEE Access*, vol. 9, pp. 35932–35946, 2021.
[32] W. Liang, Z. Ding, Y. Li, and L. Song, "User pairing for downlink non-orthogonal multiple access networks using matching algorithm," *IEEE Trans. Commun.*, vol. 65, no. 12, pp. 5319–5332, Dec. 2017.
[33] Z. Ding, P. Fan, and H. V. Poor, "Impact of user pairing on 5G nonorthogonal multiple-access downlink transmissions," *IEEE Trans. Veh. Technol.*, vol. 65, no. 8, pp. 6010–6023, Sep. 2015.
[34] M. Elhattab, M.-A. Arfaoui, C. Assi, and A. Ghrayeb, "Reconfigurable intelligent surface assisted coordinated multipoint in downlink NOMA networks," *IEEE Commun. Lett.*, vol. 25, no. 2, pp. 632–636, Feb. 2021, doi: 10.1109/LCOMM.2020.3029717.
[35] Y. Li, M. Jiang, Q. Zhang, and J. Qin, "Joint beamforming design in multi-cluster MISO NOMA reconfigurable intelligent surface-aided downlink communication networks," *IEEE Trans. Commun.*, vol. 69, no. 1, pp. 664–674, Jan. 2021, doi: 10.1109/TCOMM.2020.3032695.
[36] X. Liu, Y. Liu, Y. Chen, and H. V. Poor, "RIS enhanced massive non-orthogonal multiple access networks: Deployment and passive beamforming design," *IEEE J. Sel. Areas Commun.*, vol. 39, no. 4, pp. 1057–1071, Apr. 2021, doi: 10.1109/JSAC.2020.3018823.
[37] T. Hou, Y. Liu, Z. Song, X. Sun, and Y. Chen, "MIMO-NOMA networks relying on reconfigurable intelligent surface: A signal cancellation-based design," *IEEE Trans. Commun.*, vol. 68, no. 11, pp. 6932–6944, Nov. 2020.
[38] T. Hou, Y. Liu, Z. Song, X. Sun, Y. Chen, and L. Hanzo, "Reconfigurable intelligent surface aided NOMA networks," *IEEE J. Sel. Areas Commun.*, vol. 38, no. 11, pp. 2575–2588, Nov. 2020.
[39] D. Selimis, K. P. Peppas, G. C. Alexandropoulos, and F. I. Lazarakis, "On the performance analysis of RIS-empowered communications over Nakagami-M fading," *IEEE Commun. Lett.*, early access, Apr. 19, 2021, doi: 10.1109/LCOMM.2021.3073981.
[40] Q. Chen, M. Li, X. Yang, R. Alturki, M. D. Alshehri, and F. Khan, "Impact of residual hardware impairment on the IoT secrecy performance of RIS-assisted NOMA networks," *IEEE Access*, vol. 9, pp. 42583–42592, 2021.
[41] L. Yang, Y. Yang, M. O. Hasna, and M.-S. Alouini, "Coverage, probability of SNR gain, and DOR analysis of RIS-aided communication systems," *IEEE Wireless Commun. Lett.*, vol. 9, no. 8, pp. 1268–1272, Aug. 2020.
[42] E. Basar, M. Di Renzo, J. De Rosny, M. Debbah, M.-S. Alouini, and R. Zhang, "Wireless communications through reconfigurable intelligent surfaces," *IEEE Access*, vol. 7, pp. 116753–116773, Aug. 2019.
[43] T. Van Chien, L. T. Tu, S. Chatzinotas, and B. Ottersten, "Coverage probability and ergodic capacity of intelligent reflecting surface-enhanced communication systems," *IEEE Commun. Lett.*, vol. 25, no. 1, pp. 69–73, Jan. 2021.
[44] S. Abeywickrama, R. Zhang, Q. Wu, and C. Yuen, "Intelligent reflecting surface: Practical phase shift model and beamforming optimization," *IEEE Trans. Commun.*, vol. 68, no. 9, pp. 5849–5863, Sep. 2020.
[45] X. Yue and Y. Liu, "Performance analysis of intelligent reflecting surface assisted NOMA networks," 2020, *arXiv:2002.09907*. [Online]. Available: http://arxiv.org/abs/2002.09907
[46] J. G. Proakis and M. Salehi, *Digital Communications*, 5th ed. New York, NY, USA: McGraw-Hill, 2008.
[47] S. Kumar, "Exact evaluations of some meijer G-functions and probability of all eigenvalues real for the product of two Gaussian matrices," *J. Phys. A, Math. Theor.*, vol. 48, no. 44, Oct. 2015, Art. no. 445206.
[48] I. S. Gradshteyn and I. M. Ryzhik, *Table of Integrals, Series, and Products*, 6th ed. San Diego, CA, USA: Academic, 2000.

ANH-TU LE was born in Lam Dong, Vietnam, in 1997. He is currently pursuing the Ph.D. degree in communication and information system in field of wireless communication. He is also a Research Assistant with the WICOM Lab, which was led by Dr. D.-T. Do. He has authored or coauthored over 25 technical articles published in peer-reviewed international journals. His research interests include wireless channel modeling, NOMA, cognitive radio, and MIMO.

NHAT-DUY XUAN HA was born in Gia Lai, Vietnam, in 1996. He is currently pursuing the Ph.D. degree in communication and information system in field of wireless communication. He is also a Research Assistant with the WICOM Lab, which was led by Dr. D.-T. Do. His research interests include wireless communications, NOMA, cognitive radio, and satellite systems.

DINH-THUAN DO (Senior Member, IEEE) received the B.S., M.Eng., and Ph.D. degrees in communications engineering from Vietnam National University (VNU-HCMC), in 2003, 2007, and 2013, respectively. He was a Visiting Ph.D. Student with the Institute of Communications Engineering, National Tsing Hua University, Taiwan, from 2009 to 2010. Prior to joining Ton Duc Thang University, he was a Senior Engineer at VinaPhone Mobile Network, from 2003 to 2009. He published one textbook and five book chapters. He has authored or coauthored over 95 technical articles published in peer-reviewed international journals (SCIE) and over 100 other journals articles and conference papers. His research interests include signal processing in wireless communications networks, reconfigurable intelligent surfaces, NOMA, UAV networks, satellite systems, physical layer security, device-to-device transmission, and energy harvesting. He was a recipient of the Golden Globe Award from Vietnam Ministry of Science and Technology, in 2015 (Top 10 Talented Young Scientist in Vietnam). He received the Creative Young Medal, in 2015. He led as a lead guest editor in several special issues in peer-reviewed journals. He serves as an associate editor of four SCIE journals.

ADÃO SILVA (Member, IEEE) received the M.Sc. and Ph.D. degrees in electronics and telecommunications from the University of Aveiro, in 2002 and 2007, respectively. He is currently an Associate Professor with the DETI, University of Aveiro, where he is also a Senior Researcher at the Instituto de Telecomunicações. He has participated in several national and European projects. He has led several research projects in broadband wireless communications at the national level. His interests include multicarrier-based systems, cooperative networks, precoding, multiuser detection, and massive MIMO and millimeter wave communications. Within these research topics, he has published more than 150 technical articles in international journals and conference proceedings. He served as a member of the TPC at several international conferences. He is currently an Associate Editor of IEEE Access and *IET Signal Processing*.

SUNEEL YADAV (Member, IEEE) received the B.Tech. degree in electronics and communication engineering from the Meerut Institute of Engineering and Technology, Meerut, India, in 2008, the M.Tech. degree in digital communications from the ABV-Indian Institute of Information Technology and Management, Gwalior, India, in 2012, and the Ph.D. degree in the Discipline of Electrical Engineering, Indian Institute of Technology Indore, Indore, India, in 2016. He is currently working with the Department of Electronics and Communication Engineering, Indian Institute of Information and Technology Allahabad, Prayagraj, India, as an Assistant Professor. He is serving as a Faculty in-charge of the Mobile and Wireless Networking Laboratory (MoWiNeT), Indian Institute of Information and Technology Allahabad, Prayagraj, India. He has numerous publications in peer-reviewed journals and conferences. His current research interests include wireless relaying techniques, cooperative communications, cognitive relaying networks, device-to-device communications, reconfigurable intelligent surfaces, signal processing, physical layer security, and MIMO systems. He also served as a TPC member, the session chair, the program co-chairs, and a reviewer for various national and international conferences. He is serving as a Reviewer in a number of international journals, including the IEEE Transactions on Vehicular Technology, the IEEE Communications Letters, the IEEE Transactions on Communications, the IEEE Transactions on Information Forensics and Security, the IEEE Systems Journal, IEEE Access, the IEEE Internet of Things Journal, the IEEE Transactions on Signal and Information Processing Over Networks, and *Physical Communication*.